Science Advances
AAAS

advances.sciencemag.org/cgi/content/full/6/17/eaaz5120/DC1

Supplementary Materials for

Quantifying methane emissions from the largest oil-producing basin in the United States from space

Yuzhong Zhang*, Ritesh Gautam*, Sudhanshu Pandey, Mark Omara, Joannes D. Maasakkers, Pankaj Sadavarte, David Lyon, Hannah Nesser, Melissa P. Sulprizio, Daniel J. Varon, Ruixiong Zhang, Sander Houweling, Daniel Zavala-Araiza, Ramon A. Alvarez, Alba Lorente, Steven P. Hamburg, Ilse Aben, Daniel J. Jacob

*Corresponding author. Email: zhangyuzhong@westlake.edu.cn (Y.Z.); rgautam@edf.org (R.G.)

Published 22 April 2020, *Sci. Adv.* **6**, eaaz5120 (2020)
DOI: 10.1126/sciadv.aaz5120

This PDF file includes:

Supplementary Text

Text S1: Methods for estimating gas flaring volume

We use the nighttime fire and flare data observed by the Visible Infrared Imaging Radiometer Suite (VIIRS) instrument onboard the Suomi National Polar-Orbiting Partnership satellite to support our analysis (https://eogdata.mines.edu/download_viirs_fire.html; data access: August 1, 2019). The product Nightfire V2.1 (CLASS) is available for the period from 2012 to 2017, while the product Nightfire V3.1 (GRAVITE) is available for the period starting 2018. We select the data with retrieved flame temperature between 1400–2500 K within the study domain. Combustion in this temperature range is usually associated with gas flaring. The spatial distribution of the flaring radiant heat in Permian is presented in Figure 3 and the evolution of the flaring radiant heat is presented in fig. S1.

We also estimate the gas flaring volume in Permian between May 2018 and March 2019 following an empirical relationship with the radiant heat proposed by Elvidge et al. (*55*):

$$V = 0.0274\ RH'$$

where V is the gas flaring rate in 10^9 m^3 a^{-1} and RH' is the modified radiant heat in MW to account for the observed nonlinear relationship between flared gas volume and radiant heat (*55*). RH' for individual flares are computed as $\sigma T^4 S^\alpha$ where σ is the Stefan–Boltzmann constant (5.67×10^{-8} W m^{-2} K^{-4}), T and S are the temperature and the source area of the flare, respectively, retrieved from VIIRS observations, and $\alpha = 0.7$ is the empirical calibration exponent determined by Elvidge et al. (*55*). The average and the standard deviation of the flaring rate during the study period is computed with daily basin-level flaring rates aggregated from individual detected flares. We estimate a flaring rate of 5.9±1.2 billion m^3 a^{-1} during May 2018 and March 2019. In comparison, the operator self-reported venting and flaring in the Permian Basin is 4.5 billion m^3 a^{-1} for 2018, according to the New Mexico Oil Conservation Division (www.emnrd.state.nm.us/OCD/statistics.html) and the Texas Railroad Commission (www.rrc.state.tx.us/oil-gas/research-and-statistics/production-data/). Previous assessments show that operator self-reported flaring data are consistently lower than satellite-based observations (*15*).

We can further compute the mass of methane contained in the flared gas (M) as

$$M = m_{\mathrm{CH_4}} \gamma \frac{V}{\upsilon}$$

where υ is 0.0224 m^3 mol^{-1} under STP conditions, m_{CH4} is 16 g mol^{-1}, and γ is the fraction of methane in natural gas (~ 80% for the Permian Basin according to EPA Oil and Gas Emissions Estimation Tool Version 1.5). Methane emissions from gas flaring can then be computed as $(1-\epsilon)M$, and methane converted to CO_2 during flaring as ϵM, where ϵ is the flaring combustion efficiency. We thus estimate that 3.4±0.8 methane Tg a^{-1} is sent to flaring. Assuming a flaring efficiency between 95%-98%, this indicates direct methane emissions of 0.07-0.17 Tg a^{-1} from gas flaring, less than 6% of the total methane emission estimate based on TROPOMI data. 3.2-3.3 Tg a^{-1} methane is converted to CO_2 during flaring.

As a form of background information, there are 154,540 active wells with 6,555 new wells (< 1 year old) in the Permian Basin during the study period (May 2018 – March 2019), according to Enverus Drillinginfo (*50*). Here, active wells are defined as wells that either reported their

oil/gas production for at least six months during the study period or reported non-zero oil/gas production at the end of the study period (March 2019). While information regarding permits in the New Mexico portion of the Permian Basin is unavailable, we estimate a total of 3,364 venting and flaring permits are effective for the Texas portion of the basin during the study period, based on the data from the Texas Railroad Commission.

Text S2: Site-level emission measurements and extrapolation to the Permian Basin

We provide here details of recent ground-based measurements and their extrapolation that were used to construct an alternative measurement-based bottom-up inventory for the Permian Basin, as an input to the atmospheric inversion modeling. The methodology and results were made publicly available in April 2019 via Environmental Defense Fund's New Mexico oil and gas pollution study (*52*). The resulting emission inventory dataset (EI_{ME} inventory) is publicly available for our study region encompassing the entire Permian Basin (DOI: https://doi.org/10.7910/DVN/NWQGHU).

Here, we provide a summary of the measurements, methodology and results. Ground-based site-level methane emission measurements at 93 oil and gas production sites in the Permian Basin were performed in July and August 2018 with a stationary downwind plume measurement technique (OTM-33A) (*52*), in which methane concentration measurements were taken downwind of target sites at 0.5 Hz using a Picarro cavity-ring down spectrometer (Model G2204). OTM-33A is a well-established emission rate quantification method that utilizes stationary downwind measurements coupled with Gaussian plume dispersion modeling to estimate site-level methane leak rates. Previous controlled release tests indicated a 95% confidence interval of +/-56% on mean site-level emissions quantified using the OTM-33A methodology (with a -10% bias) (*56*).

The sampling was carried out predominantly in the New Mexico portion of the Permian Basin, following a stratified random sampling approach to account for the wide diversity of well age within the oil producing fields. Final site selection at a particular field was determined by local meteorology on the day of measurements as well as access to public roads downwind of target sites. A FLIR optical gas-imaging camera is used to identify major emission sources such as storage tanks and to facilitate positioning of the vehicle within the plume.

In this study, sites were recorded as below the detection limit (BDL) if no clear plume was detected downwind. The BDL was estimated at 0.04 kg/h based on previous work (*56*). In total, 52 sites were reported to have BDL emissions while 41 sites had emissions that were above the detection limit. The detectability of emissions from a site are found to be closely associated with the complexity of infrastructure. Emissions were below the detection limit (0.04 kg/h/site) for over 90% of "simple" sites (with only wellheads and/or pump jacks), but were detectable for most (78%) "complex" sites (also with storage tanks and/or compressors). We determine the site-level emission factor for "simple" sites to be 0.04 kg/h/site and that for "complex" sites to be 5.2 kg/h/site. For the latter, a lower bound estimate following the procedure described in Zavala-Araiza et al. (*57*) (5.2–79 kg CH_4/h/site) is used here for a conservatively low estimate.

To extrapolate to basin-level emissions based on the above measurements, we need to estimate the number of "simple" vs. "complex" sites in Permian. We used satellite imagery data from Google Maps to perform manual classification ("simple", "complex", or "unknown") of 25,000 well sites in the New Mexico portion of the Delaware Basin. Human classification of well site images was achieved via a crowdsourcing marketplace—Amazon Mechanical Turk (https://www.mturk.com/). Depending on the observed equipment on site, each image representing a well site location was manually classified by five workers as either a "simple" site, a "complex" site, or a site of "unknown" configuration. A site's final classification was

determined based on at least a 60% agreement among the workers. On average, 33% of the sites were classified as “complex” sites and 58% were classified as “simple” sites, with the remainder (8.6%) being sites of “unknown” configuration. We assume this distribution for the New Mexico portion of the Delaware Basin applies to the whole Permian Basin and count the “unknown” category as “simple”. We therefore estimate that the numbers for “simple” and “complex” sites are 97,000 and 48,600, respectively. Combining site classifications with corresponding site-level emission factors leads to an estimate of 2.3 Tg a^{-1} for methane emissions from O/G production in the Permian Basin.

Text S3 Mass balance method for emission quantification

As an independent comparison of our inverse modeling results, we apply the mass balance method of Buchwitz et al. (*23*) to derive the average methane emission rate over the Permian Basin (30-34 °N, 101-105 °W). This data-driven approach does not require prior emissions and atmospheric transport model, and therefore is a fast algorithm, compared to atmospheric inversion. With large amount of high resolution observations delivered by satellite instruments such as TROPOMI, the method has potential as a quick screening and assessment tool for quantifying regional annual methane emissions.

Here, we apply the method to the elevation corrected methane column XCH_4^t data from May 2018 – March 2019 regridded to 0.2° × 0.2° (Figure 1). The emission rate (Q, Tg yr^{-1}) is computed by applying a conversion factor (CF) to the XCH_4^t enhancement (ΔXCH_4^t, ppbv, computed as mean XCH_4^t in the source region minus mean XCH_4^t in the surrounding background) as follows (*23*):

$$Q = \Delta XCH_4^t \times CF$$

$$CF = L \times V \times M_{exp} \times M \times C$$

where L is the effective length of the source area (computed as square root of the source area, 375 km) through which wind of effective speed V (17 km hr^{-1}) ventilates the air parcel carrying emitted methane, M_{exp} is the ratio of average surface pressure in the region (898.32 hPa for Permian) and standard surface pressure of 1013.25 hPa, M is a constant to convert mole fraction to mass change per area (5.345 kg CH_4 km^{-2} ppb^{-1}) in standard atmospheric conditions, and C is a dimensionless factor chosen to be 2.0, derived by Buchwitz et al. (*23*), based on the concentration difference of the air parcel before and after entering the source area. The surrounding background is defined as a rectangular box centered at the Permian Basin. We vary the width and length of the surrounding background from 8 to 24 degrees at a 2-degree interval. Wind speed V is taken from the average horizontal boundary layer winds over the source region from ECMWF ERA5 data at 20:00 UTC, which is close to TROPOMI overpass time over Permian basin. Using the mass balance method, we estimate an annual average methane emission rate of 3.2 Tg a^{-1} from the Permian Basin.

The uncertainty of the method (σ_{tot}) is computed as $\sqrt{\sigma^2_{\Delta XCH_4^t} + \sigma^2_{\mathrm{CF}}}$ to account for contributions from both ΔXCH_4^t and CF. The uncertainty due to ΔXCH_4^t ($\sigma_{\Delta XCH_4^t}$), dominated by the variations in the background XCH_4^t, is estimated by varying the size of surrounding background region. The uncertainty due to CF (σ_{CF}), primarily contributed by the uncertainty in wind speed, is computed using the empirical equation derived in Buchwitz et al. (*23*) We find σ_{tot} to be 2.0 Tg a^{-1} ($\sigma_{\Delta XCH_4^t}$ = 0.5 Tg a^{-1} and σ_{CF} = 1.9 Tg a^{-1}) in this work.

Text S4 Current status of regulation in the Permian Basin

Oil and gas production on federal lands occur only on the New Mexico portion of the Permian Basin. These lands accounted for 9.6% (398 Bcf) and 8.9% (18 Bcf) of total Permian gas production (https://www.enverus.com/) and gas flaring (https://eogdata.mines.edu/download_global_flare.html), respectively. With the rescinding of the gas capture and fugitive emissions requirements in the BLM's 2016 Methane Waste Prevention Rule, Permian Basin operators with assets on both federal and state lands are now required to meet the state standards only. Both New Mexico and Texas do not have associated gas capture targets and both states permit associated gas flaring in the Permian Basin. Additionally, both states currently do not directly regulate oil and gas methane emissions.

In 2016, the Bureau of Land Management's Methane Waste Prevention Rule (https://www.regulations.gov/document?D=BLM-2016-0001-9126) imposed limits on associated gas venting, flaring and fugitive leaks from new and existing sites operated on federal lands. The BLM's 2018 revision (https://www.govinfo.gov/content/pkg/FR-2018-09-28/pdf/2018-20689.pdf) of the 2016 rule rescinded these requirements, arguing that these rules were unnecessary because the EPA had analogous requirements for fugitive leaks, and venting and flaring are regulated under state requirements. However, the EPA fugitive emissions requirements are less stringent—they focus only on new or modified facilities commissioned in September 2015 and later and do not address gas waste from other existing sites. Furthermore, the EPA recently proposed to revise these requirements (https://www.federalregister.gov/documents/2018/10/15/2018-20961/oil-and-natural-gas-sector-emission-standards-for-new-reconstructed-and-modified-sources), loosening the leak detection and repair frequency and allowing more time to perform repairs of detected leaks. Thus, the vast majority of Permian operations (i.e. existing sites) on both federal and state lands are now required to meet the state standards only.

Both New Mexico and Texas do not have associated gas capture requirements analogous to the requirements in the 2016 BLM rule, and both states currently permit associated gas flaring in the Permian Basin. The Texas Railroad Commission's Statewide Rule 32 (https://texreg.sos.state.tx.us/public/readtac$ext.TacPage?sl=R&app=9&p_dir=&p_rloc=&p_tloc=&p_ploc=&pg=1&p_tac=&ti=16&pt=1&ch=3&rl=32) grants administrative flaring permits that can be renewed for 180 days. Operators can apply for extension to flare beyond the first 180 days and provide additional information on progress made "toward establishing the necessary infrastructure to produce gas rather than flare it." These extensions are routinely granted, primarily because "the operator is waiting for pipeline construction scheduled to be completed by a specified date." Similarly, The New Mexico Administrative Code 19.15.18.12A (http://164.64.110.134/parts/title19/19.015.0018.html) permits venting and flaring of casing-head gas in unlimited quantities within the first 60 days following completion. Exceptions may be granted beyond the first 60 days when venting/flaring appears "reasonably necessary to protect correlative rights, prevent waste or prevent undue hardships on the applicant."

Supplementary figures

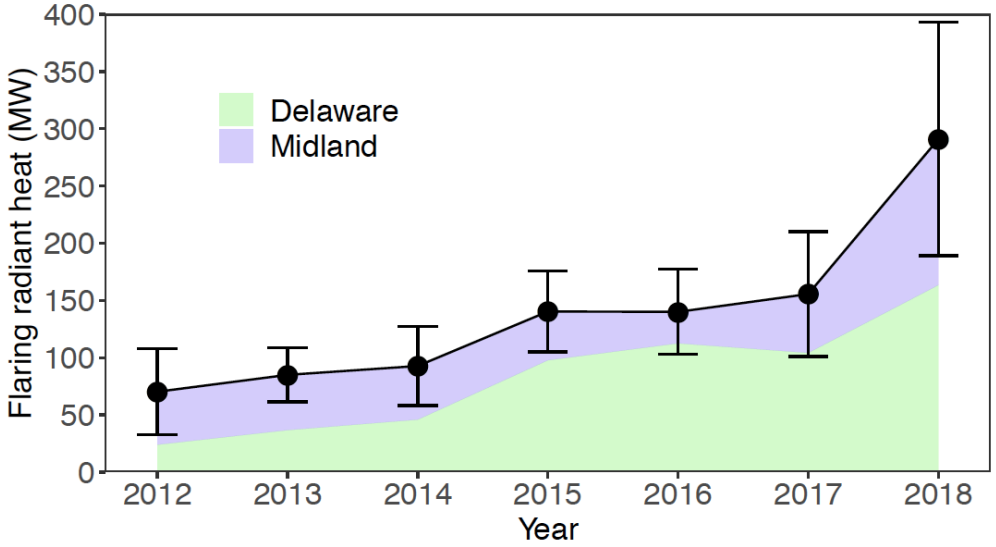

Fig. S1 Annual mean gas flaring radiant heat over the Permian Basin observed by VIIRS from 2012 to 2018. Error bars represent the standard deviation of monthly variations. The blue shading represents the Midland Basin and the green shading the Delaware Basin.

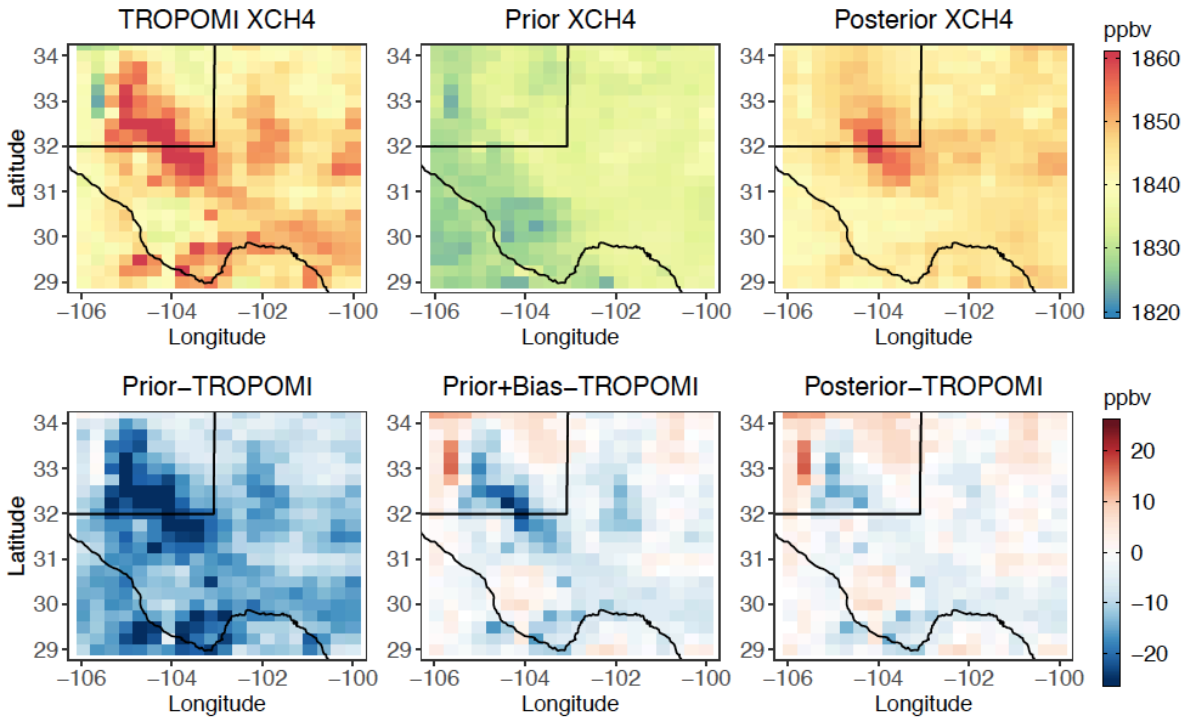

Fig. S2 Observed and simulated XCH_4 over the Permian Basin. The top panels show TROPOMI observations, GEOS-Chem prior simulation, and GEOS-Chem posterior simulation respectively. The bottom panels show the difference between simulations (prior simulation, prior simulation with regional biases corrected, and posterior simulation) and observations. Data are averaged from May 2018 to March 2019.

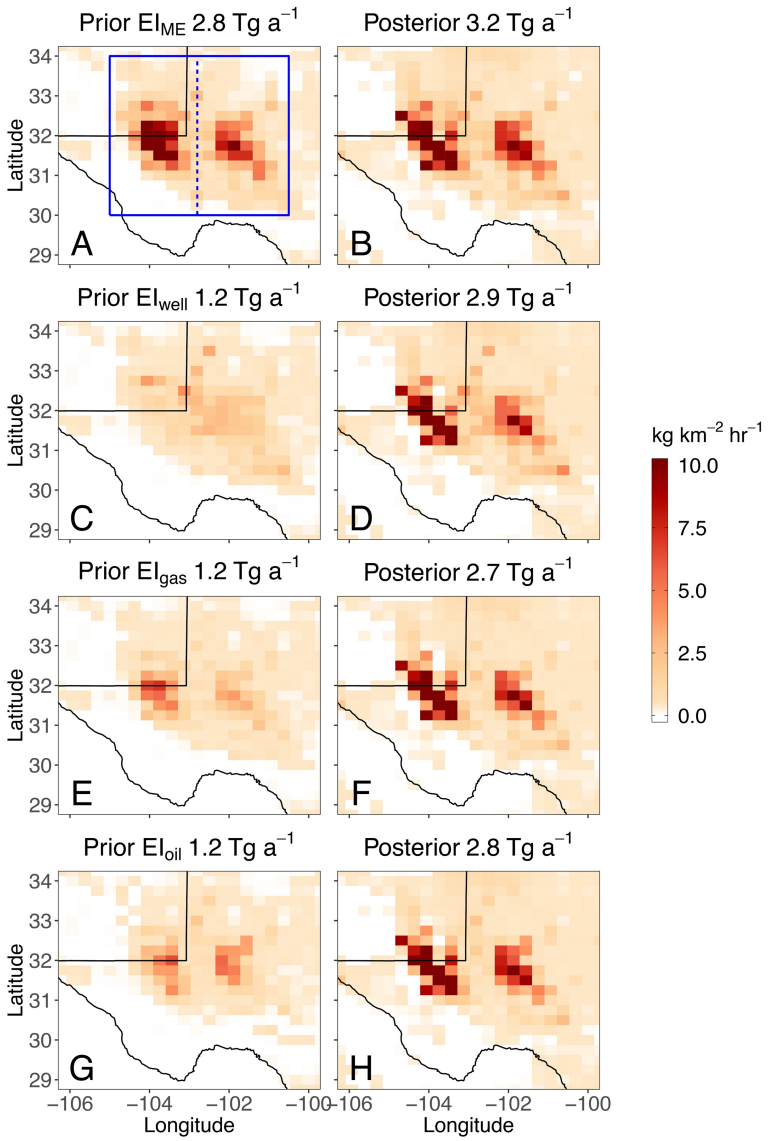

Fig. S3 Spatial distribution of methane emission rates in the Permian Basin in alternative prior emission inventories (A, C, E, G) and the corresponding posterior estimates (B, D, F, H). A, B are for EI_{ME}, C, D for EI_{well}, E, F for EI_{gas}, and G, H for EI_{oil}. The solid blue box encloses the Permian Basin with the two sub-basins to the left (the Delaware) and the right (the Midland) of the dashed line.

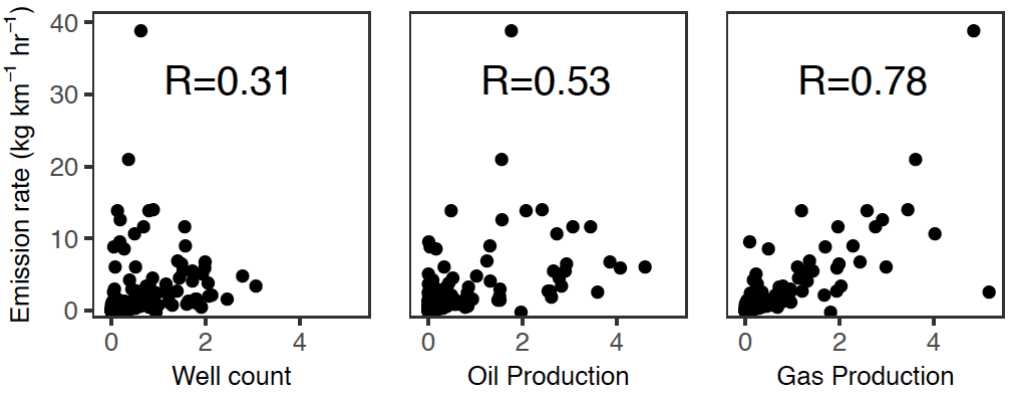

Fig. S4 Spatial correlation between the posterior methane emission rates and O/G production activities for each grid cell. Data for well count, oil production, and gas production are normalized and expressed in %.

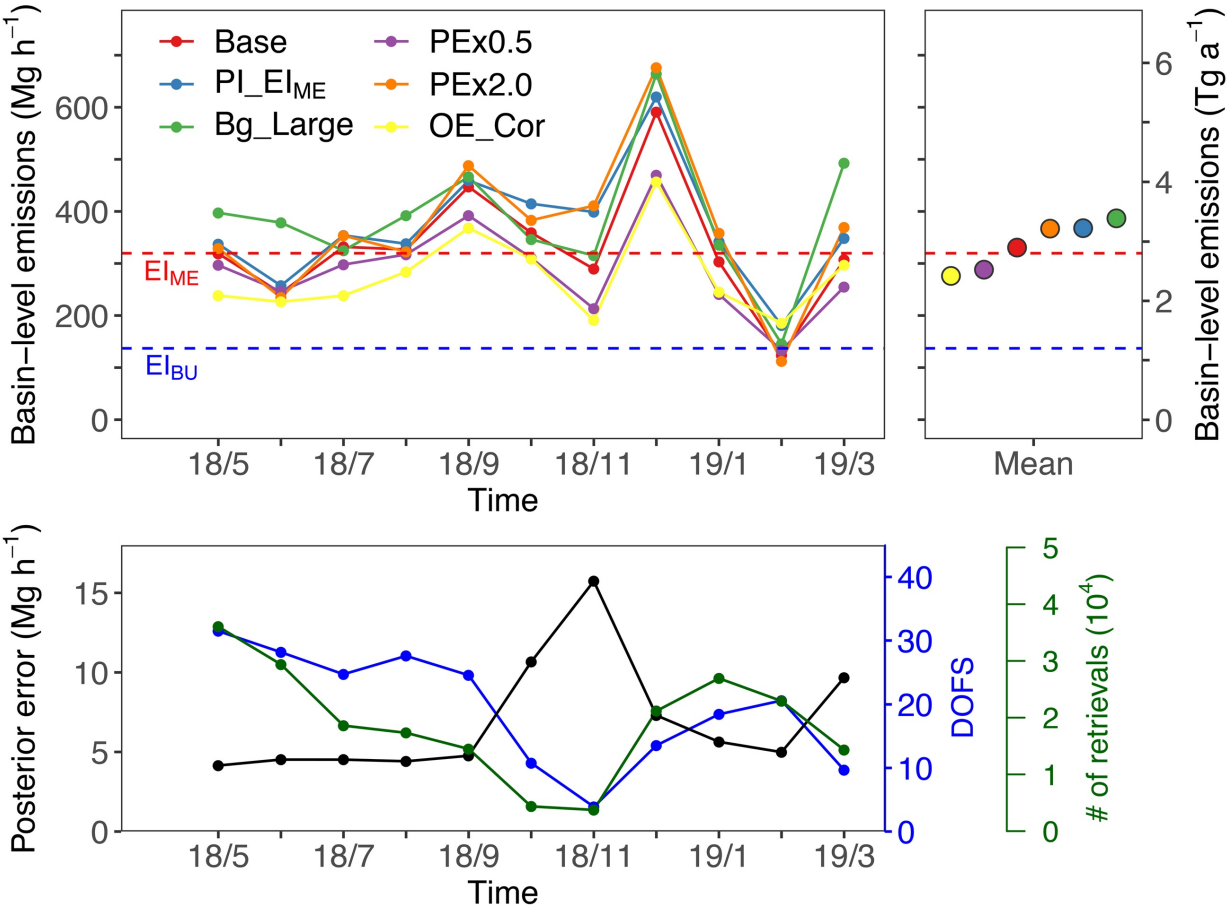

Fig. S5 Monthly methane emission rates estimated by the base and sensitivity inversions (top) and analytical posterior error (bottom). The top panel shows the monthly and mean basin-level methane emission estimates by the base and sensitivity inversions (table S2). Blue and red dashed lines indicate basin-level emissions estimated by EI_{BU} and EI_{ME}, respectively. The bottom panel shows monthly count of successful retrievals used in the base inversion (green), analytical posterior errors for the basin-level methane emissions (black), and corresponding degrees-of-freedom for signals (DOFS) (blue).

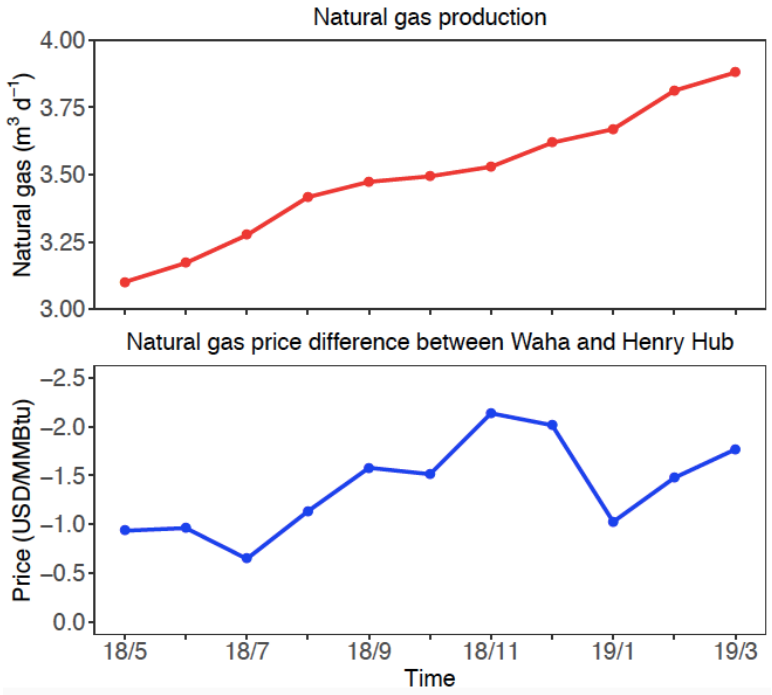

Fig. S6 Monthly natural gas production and price in the Permian Basin. Top: natural gas production in the Permian Basin. Bottom: monthly mean natural gas spot price between Waha (in the Permian Basin) and Henry Hub (benchmark of the North America natural gas market). Note that the price differences (Waha – Henry Hub) are negative, meaning that natural gas is traded below the Henry Hub benchmark within the Permian Basin.

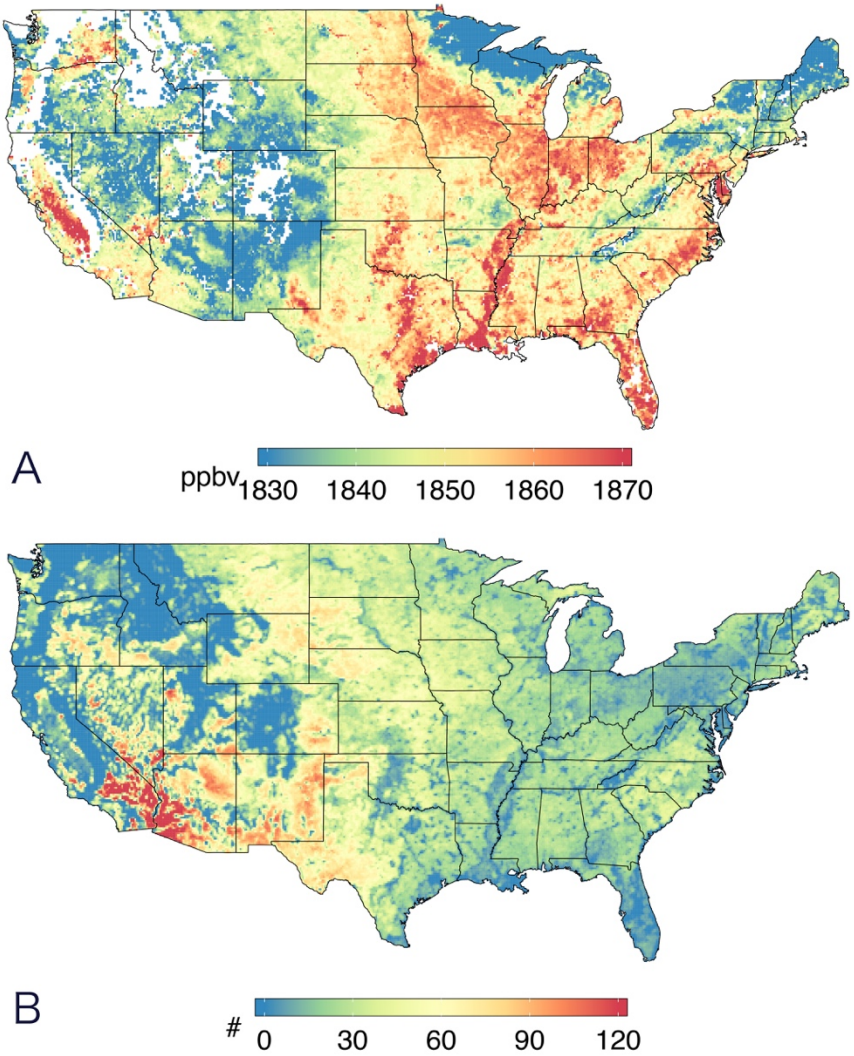

Fig. S7 TROPOMI XCH4 observations over the conterminous U.S. (A) Average column methane mixing ratio (XCH_4) over the conterminous U.S. during the study period. The 11-month average is derived from monthly mean XCH_4 from TROPOMI. (B) Number of days with successful retrievals on the 0.2°×0.2° grid from May 2018 to March 2019.

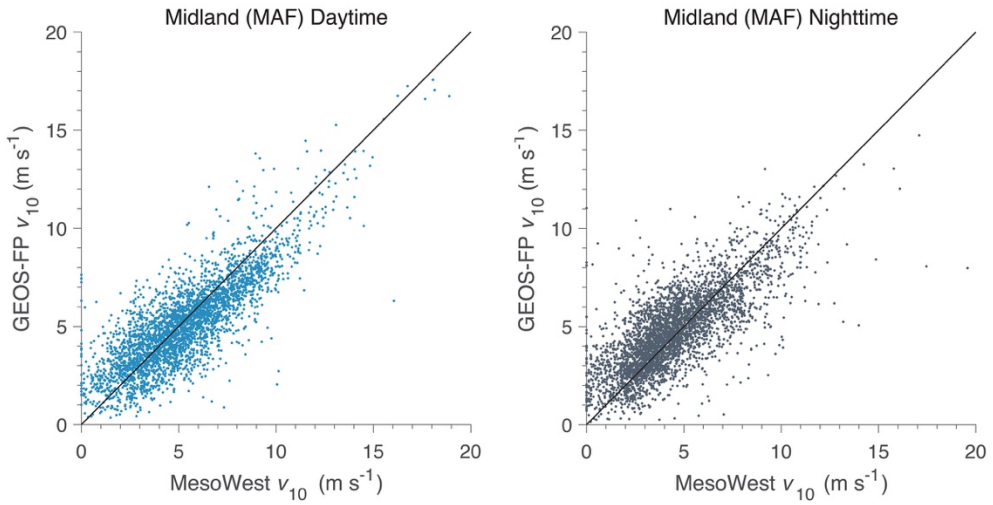

Fig. S8 Evaluation of GEOS-FP wind speed in daytime (left) and nighttime (right). Data are from May 2018 to March 2019. Surface measurements at the Midland Airport (MAF) in the Permian Basin are obtained from MesoWest (mesowest.utah.edu).

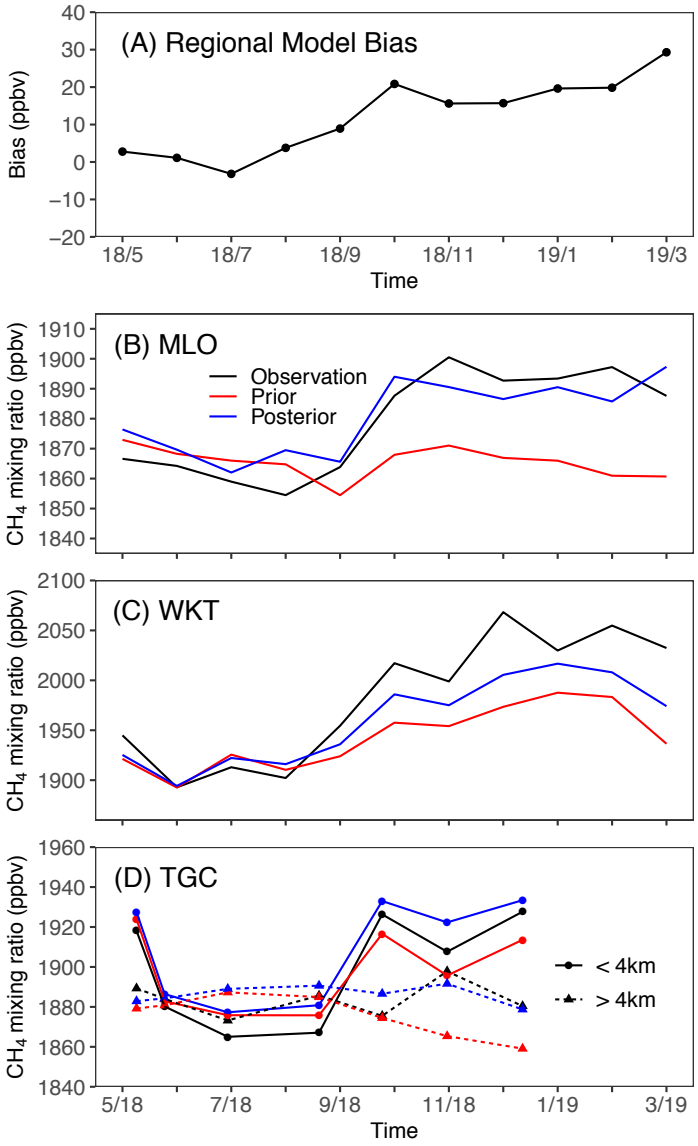

Fig. S9 Regional model biases inferred from the TROPOMI inversion and evaluation with independent observations. (A) monthly regional model biases for the simulated methane column (XCH_4) from the base inversion. (B-D) Evaluation with surface measurements at MLO (B), tower measurements at WKT (C), and aircraft vertical profile measurements ~ 250–8000 m at TGC (D). The bias corrected model results (blue) are computed as the sum of original model results (red) and model biases inferred from the inversion (regional model biases derived from our inversion times a factor of 1.25 to convert the column bias to the free tropospheric bias). We show monthly averages for MLO and WKT, and flight averages above and below 4 km altitude for TGC. This comparison suggests that the regional model bias term introduced in the inversion is effective for correcting background biases resulting mainly from imperfect boundary conditions.

Supplementary tables

Table S1. Estimates of O/G-related methane emissions reported in previous aircraft-based studies for 11 U.S. O/G producing basins. [a]

	Ref.	Date Sampled (Month/year)	NG production (10^9 m^3 a^{-1})	CH_4 fraction in NG (%)	O/G-related emissions (Tg a^{-1})	Production normalized emission rate (%)
Haynesville	(*26*)	6/2013	80	86	0.63	1.3
Barnett	(*27*)	3 & 10/2013	61	89	0.53	1.4
NE PA	(*28*)	5/2015	60	95	0.16	0.4
NE PA	(*26*)	7/2013	N/A	95	0.11	0.3
San Juan	(*12*)	4/2015	29	83	0.50	3.0
Fayetteville	(*29*)	10/2015	26	97	0.24	1.4
Fayetteville	(*26*)	7/2013	N/A	97	0.31	1.9
Bakken	(*30*)	5/2014	20	47	0.24	3.7
Uinta	(*31*)	2/2012	12	89	0.48	6.6
Denver Basin	(*32*)	5/2012	10	79	0.17	3.1
West Arkoma	(*26*)	7/2013	4	96	0.23	9.1
Bakken	(*24*)	4/2015	13	47	0.25	5.4
Barnett	(*24*)	4/2015	44	87	0.40	1.5
Denver Basin	(*24*)	3/2015	14	77	0.16	2.1
Eagle Ford [b]	(*24*)	4/2015	56	N/A	0.73	2.5
west			32	77	0.36	2.0
east			24	68	0.37	3.2
Haynesville	(*24*)	4/2015	54	90	0.37	1.0
SW PA	(*25*)	8 & 9/2015	29	88	0.19	1.1
11-basin sum [c]			322	N/A	3.71	1.9
Permian	This study	5/2018-3/2019	128	80	2.7	3.7

[a] Data are taken from a summary by Alvarez et al. (*7*) except for those from Peischl et al. (*24*) and Ren et al. (*25*).

[b] Emissions from Eagle Ford are reported separately as west and east sub-basins (*24*), based on which we compute the data for the entire basin.

[c] 11-basin sum is computed with latest measurements if multiple studies exist for a specific basin. Therefore, shaded rows are excluded in calculating the 11-basin sum.

Table S2. Total basin-level methane emission estimates from an ensemble of sensitivity inversions perturbing a variety of inversion parameters.

	Inversion	Basin methane emissions ($Tg\ a^{-1}$)
	Base inversion [a]	2.9
	Sensitivity inversions perturbing prior emissions [b]	
PI_EI_{ME}	EI_{ME} as prior emissions	3.2
PI_EI_{oil}	EI_{oil} as prior emissions	2.7
PI_EI_{gas}	EI_{gas} as prior emissions	2.7
PI_EI_{well}	EI_{well} as prior emissions	2.9
	Sensitivity inversions perturbing the size of spatial domain	
Bg_Large	27°–36°N, 98°–108° W	3.4
	Sensitivity inversions perturbing error covariance specifications	
PE×2	Double prior error	3.2
PE×0.5	Halve prior error	2.5
OE_Cor	Specify observational error correlations [c]	2.4

[a] Base inversion is performed over a domain in 29°–34°N, 100°–106° W and uses EI_{BU} as prior information. Both $\mathbf{S}_O$ and $\mathbf{S}_A$ are taken to be diagonal. Prior errors are specified as the absolute difference between EI_{BU} and EI_{ME}. Observational errors are specified following the residual error method (*43*).

[b] Spatial distributions of these prior emission inventories and corresponding posterior estimates are shown in fig. S3.

[c] $\mathbf{S}_O$ is specified following Cusworth et al. (*44*) by assuming 4 ppbv model errors with a spatial correlation length of 40 km and independent instrument errors.

REFERENCES AND NOTES

1. D. Shindell, J. C. I. Kuylenstierna, E. Vignati, R. van Dingenen, M. Amann, Z. Klimont, S. C. Anenberg, N. Muller, G. Janssens-Maenhout, F. Raes, J. Schwartz, G. Faluvegi, L. Pozzoli, K. Kupiainen, L. Höglund-Isaksson, L. Emberson, D. Streets, V. Ramanathan, K. Hicks, N. T. K. Oanh, G. Milly, M. Williams, V. Demkine, D. Fowler, Simultaneously mitigating near-term climate change and improving human health and food security. *Science* **335**, 183–189 (2012).
2. G. Myhre, D. Shindell, F.-M. Bréon, W. Collins, J. Fuglestvedt, J. Huang, D. Koch, J.-F. Lamarque, D. Lee, B. Mendoza, T. Nakajima, A. Robock, G. Stephens, T. Takemura, H. Zhang, Anthropogenic and natural radiative forcing, in *Climate Change 2013: The Physical Science Basis. Contribution of Working Group I to the Fifth Assessment Report of the Intergovernmental Panel on Climate Change*, T. F. Stocker, D. Qin, G.-K. Plattner, M. Tignor, S. K. Allen, J. Boschung, A. Nuales, Y. Xia, V. Bex, P. M. Midgley, Eds. (Cambridge Univ. Press, 2013), pp. 659–740.
3. J. D. Maasakkers, D. J. Jacob, M. P. Sulprizio, T. R. Scarpelli, H. Nesser, J.-X. Sheng, Y. Zhang, M. Hersher, A. A. Bloom, K. W. Bowman, J. R. Worden, G. Janssens-Maenhout, R. J. Parker, Global distribution of methane emissions, emission trends, and OH concentrations and trends inferred from an inversion of GOSAT satellite data for 2010–2015. *Atmos. Chem. Phys.* **19**, 7859–7881 (2019).
4. S. Schwietzke, O. A. Sherwood, L. M. P. Bruhwiler, J. B. Miller, G. Etiope, E. J. Dlugokencky, S. E. Michel, V. A. Arling, B. H. Vaughn, J. W. C. White, P. P. Tans, Upward revision of global fossil fuel methane emissions based on isotope database. *Nature* **538**, 88–91 (2016).
5. B. Hmiel, V. V. Petrenko, M. N. Dyonisius, C. Buizert, A. M. Smith, P. F. Place, C. Harth, R. Beaudette, Q. Hua, B. Yang, I. Vimont, S. E. Michel, J. P. Severinghaus, D. Etheridge, T. Bromley, J. Schmitt, X. Faïn, R. F. Weiss, E. Dlugokencky, Preindustrial $^{14}CH_4$ indicates greater anthropogenic fossil CH_4 emissions. *Nature* **578**, 409–412 (2020).
6. R. A. Alvarez, S. W. Pacala, J. J. Winebrake, W. L. Chameides, S. P. Hamburg, Greater focus needed on methane leakage from natural gas infrastructure. *Proc. Natl. Acad. Sci. U.S.A.* **109**, 6435–6440 (2012).
7. R. A. Alvarez, D. Zavala-Araiza, D. R. Lyon, D. T. Allen, Z. R. Barkley, A. R. Brandt, K. J. Davis, S. C. Herndon, D. J. Jacob, A. Karion, E. A. Kort, B. K. Lamb, T. Lauvaux, J. D. Maasakkers, A. J. Marchese, M. Omara, S. W. Pacala, J. Peischl, A. L. Robinson, P. B. Shepson, C. Sweeney, A. Townsend-Small, S. C. Wofsy, S. P. Hamburg, Assessment of methane emissions from the U.S. oil and gas supply chain. *Science* **361**, 186–188 (2018).
8. EPA, Inventory of US greenhouse gas emissions and sinks: 1990–2015 (2017); https://www.epa.gov/ghgemissions/inventory-us-greenhouse-gas-emissions-and-sinks-1990-2015.

9. D. J. Jacob, A. J. Turner, J. D. Maasakkers, J. Sheng, K. Sun, X. Liu, K. Chance, I. Aben, J. McKeever, C. Frankenberg, Satellite observations of atmospheric methane and their value for quantifying methane emissions. *Atmos. Chem. Phys.* **16**, 14371–14396 (2016).
10. E. A. Kort, C. Frankenberg, K. R. Costigan, R. Lindenmaier, M. K. Dubey, D. Wunch, Four corners: The largest US methane anomaly viewed from space. *Geophys. Res. Lett.* **41**, 6898–6903 (2014).
11. C. Frankenberg, A. K. Thorpe, D. R. Thompson, G. Hulley, E. A. Kort, N. Vance, J. Borchardt, T. Krings, K. Gerilowski, C. Sweeney, S. Conley, B. D. Bue, A. D. Aubrey, S. Hook, R. O. Green, Airborne methane remote measurements reveal heavy-tail flux distribution in Four Corners region. *Proc. Natl. Acad. Sci. U.S.A.* **113**, 9734–9739 (2016).
12. M. L. Smith, A. Gvakharia, E. A. Kort, C. Sweeney, S. A. Conley, I. Faloona, T. Newberger, R. Schnell, S. Schwietzke, S. Wolter, Airborne quantification of methane emissions over the four corners region. *Environ. Sci. Technol.* **51**, 5832–5837 (2017).
13. EIA, Drilling productivity report; https://www.eia.gov/petroleum/drilling/ [accessed 1 May 2019].
14. C. Krauss, "The 'monster' Texas oil field that made the U.S. a star in the world market," *New York Times*, 2019.
15. K. A. Willyard, G. W. Schade, Flaring in two Texas shale areas: Comparison of bottom-up with top-down volume estimates for 2012 to 2015. *Sci. Total Environ.* **691**, 243–251 (2019).
16. SRON, S5P Mission Performance Centre Methane [L2__CH4___] Readme, S5P-MPC-SRON-PRF-CH4, V01.03.02 (2019).
17. J. P. Veefkind, I. Aben, K. McMullan, H. Förster, J. de Vries, G. Otter, J. Claas, H. J. Eskes, J.F. de Haan, Q. Kleipool, M. van Weele, O. Hasekamp, R. Hoogeveen, J. Landgraf, R. Snel, P. Tol, P. Ingmann, R. Voors, B. Kruizinga, R. Vink, H. Visser, P.F. Levelt, TROPOMI on the ESA Sentinel-5 Precursor: A GMES mission for global observations of the atmospheric composition for climate, air quality and ozone layer applications. *Remote Sens. Environ.* **120**, 70–83 (2012).
18. EIA, The Wolfcamp play has been key to Permian Basin oil and natural gas production growth (2018); https://www.eia.gov/todayinenergy/detail.php?id=37532#tab1 [accessed 18 August 2019].
19. Y. Zhang, R. Gautam, D. Zavala-Araiza, D. J. Jacob, R. Zhang, L. Zhu, J.-X. Sheng, T. Scarpelli, Satellite-observed changes in Mexico's offshore gas flaring activity linked to oil/gas regulations. *Geophys. Res. Lett.* **46**, 1879–1888 (2019).
20. B. N. Duncan, L. N. Lamsal, A. M. Thompson, Y. Yoshida, Z. Lu, D. G. Streets, M. M. Hurwitz, K. E. Pickering, A space-based, high-resolution view of notable changes in urban NO_x pollution around the world (2005-2014). *J. Geophys. Res. Atmos.* **121**, 976–996 (2016).

21. J. X. Sheng, D. J. Jacob, A. J. Turner, J. D. Maasakkers, M. P. Sulprizio, A. A. Bloom, A. E. Andrews, D. Wunch, High-resolution inversion of methane emissions in the Southeast US using SEAC^{4}RS aircraft observations of atmospheric methane: Anthropogenic and wetland sources. *Atmos. Chem. Phys.* **18**, 6483–6491 (2018).
22. EPA, Inventory of US greenhouse gas emissions and sinks: 1990–2017 (2019); https://www.epa.gov/ghgemissions/inventory-us-greenhouse-gas-emissions-and-sinks-1990-2017.
23. M. Buchwitz, O. Schneising, M. Reuter, J. Heymann, S. Krautwurst, H. Bovensmann, J. P. Burrows, H. Boesch, R. J. Parker, P. Somkuti, R. G. Detmers, O. P. Hasekamp, I. Aben, A. Butz, C. Frankenberg, A. J. Turner, Satellite-derived methane hotspot emission estimates using a fast data-driven method. *Atmos. Chem. Phys.* **17**, 5751–5774 (2017).
24. J. Peischl, S. J. Eilerman, J. A. Neuman, K. C. Aikin, J. de Gouw, J. B. Gilman, S. C. Herndon, R. Nadkarni, M. Trainer, C. Warneke, T. B. Ryerson,Quantifying methane and ethane emissions to the atmosphere from Central and Western U.S. oil and natural gas production regions. *J. Geophys. Res. Atmos.* **123**, 7725–7740 (2018).
25. X. Ren, D. L. Hall, T. Vinciguerra, S. E. Benish, P. R. Stratton, D. Ahn, J. R. Hansford, M. D. Cohen, S. Sahu, H. He, C. Grimes, J. D. Fuentes, P. B. Shepson, R. J. Salawitch, S. H. Ehrman, R. R. Dickerson, Methane emissions from the Marcellus Shale in Southwestern Pennsylvania and Northern West Virginia based on airborne measurements. *J. Geophys. Res. Atmos.* **124**, 1862–1878 (2019).
26. J. Peischl, T. B. Ryerson, K. C. Aikin, J. A. de Gouw, J. B. Gilman, J. S. Holloway, B. M. Lerner, R. Nadkarni, J. A. Neuman, J. B. Nowak, M. Trainer, C. Warneke, D. D. Parrish, Quantifying atmospheric methane emissions from the Haynesville, Fayetteville, and northeastern Marcellus shale gas production regions. *J. Geophys. Res. Atmos.* **120**, 2119–2139 (2015).
27. A. Karion, C. Sweeney, E. A. Kort, P. B. Shepson, A. Brewer, M. Cambaliza, S. A. Conley, K. Davis, A. Deng, M. Hardesty, S. C. Herndon, T. Lauvaux, T. Lavoie, D. Lyon, T. Newberger, G. Pétron, C. Rella, M. Smith, S. Wolter, T. I. Yacovitch, P. Tans, Aircraft-based estimate of total methane emissions from the Barnett Shale region. *Environ. Sci. Technol.* **49**, 8124–8131 (2015).
28. Z. R. Barkley, T. Lauvaux, K. J. Davis, A. Deng, N. L. Miles, S. J. Richardson, Y. Cao, C. Sweeney, A. Karion, M. K. Smith, E. A. Kort, S. Schwietzke, T. Murphy, G. Cervone, D. Martins, J. D. Maasakkers, Quantifying methane emissions from natural gas production in north-eastern Pennsylvania. *Atmos. Chem. Phys.* **17**, 13941–13966 (2017).
29. S. Schwietzke, G. Pétron, S. Conley, C. Pickering, I. Mielke-Maday, E. J. Dlugokencky, P. P. Tans, T. Vaughn, C. Bell, D. Zimmerle, S. Wolter, C. W. King, A. B. White, T. Coleman, L. Bianco, R. C.

Schnell, Improved mechanistic understanding of natural gas methane emissions from spatially resolved aircraft measurements. *Environ. Sci. Technol.* **51**, 7286–7294 (2017).

30. J. Peischl, A. Karion, C. Sweeney, E. A. Kort, M. L. Smith, A. R. Brandt, T. Yeskoo, K. C. Aikin, S. A. Conley, A. Gvakharia, M. Trainer, S. Wolter, T. B. Ryerson, Quantifying atmospheric methane emissions from oil and natural gas production in the Bakken shale region of North Dakota. *J. Geophys. Res. Atmos.* **121**, 6101–6111 (2016).
31. A. Karion, C. Sweeney, G. Pétron, G. Frost, R. Michael Hardesty, J. Kofler, B. R. Miller, T. Newberger, S. Wolter, R. Banta, A. Brewer, E. Dlugokencky, P. Lang, S. A. Montzka, R. Schnell, P. Tans, M. Trainer, R. Zamora, S. Conley, Methane emissions estimate from airborne measurements over a western United States natural gas field. *Geophys. Res. Lett.* **40**, 4393–4397 (2013).
32. G. Pétron, A. Karion, C. Sweeney, B. R. Miller, S. A. Montzka, G. J. Frost, M. Trainer, P. Tans, A. Andrews, J. Kofler, D. Helmig, D. Guenther, E. Dlugokencky, P. Lang, T. Newberger, S. Wolter, B. Hall, P. Novelli, A. Brewer, S. Conley, M. Hardesty, R. Banta, A. White, D. Noone, D. Wolfe, R. Schnell, A new look at methane and nonmethane hydrocarbon emissions from oil and natural gas operations in the Colorado Denver-Julesburg Basin. *J. Geophys. Res. Atmos.* **119**, 6836–6852 (2014).
33. M. Omara, M. R. Sullivan, X. Li, R. Subramanian, A. L. Robinson, A. A. Presto, Methane emissions from conventional and unconventional natural gas production sites in the marcellus shale basin. *Environ. Sci. Technol.* **50**, 2099–2107 (2016).
34. RBN Energy, "Hell In Texas—Permian gas takeaway headed for capacity wall," RBN Energy Drill Down Report (2018).
35. EIA, Natural gas consumption by end use; https://www.eia.gov/dnav/ng/ng_cons_sum_dcu_STX_a.htm. [accessed 20 August 2019].
36. M. Etminan, G. Myhre, E. J. Highwood, K. P. Shine, Radiative forcing of carbon dioxide, methane, and nitrous oxide: A significant revision of the methane radiative forcing. *Geophys. Res. Lett.* **43**, 12,614–12,623 (2016).
37. T. Curtis, B. Montalbano, *The Permian Basin Produces Gas, Too—Permian Basin Oil and Gas Production Growth: A Case Study for Gas Infrastructure Needs in the U.S.* (Energy Policy Research Foundation Inc., 2018).
38. H. Hu, J. Landgraf, R. Detmers, T. Borsdorff, J. aan de Brugh, I. Aben, A. Butz, O. Hasekamp, Toward global mapping of methane with TROPOMI: First results and intersatellite comparison to GOSAT. *Geophys. Res. Lett.* **45**, 3682–3689 (2018).

39. H. Hu, O. Hasekamp, A. Butz, A. Galli, J. Landgraf, J. Aan de Brugh, T. Borsdorff, R. Scheepmaker, I. Aben, The operational methane retrieval algorithm for TROPOMI. *Atmos. Meas. Tech.* **9**, 5423–5440 (2016).
40. O. Hasekamp, A. Lorente, H. Hu, A. Butz, J. aan de Brugh, J. Landgraf, "Algorithm theoretical baseline document for Sentinel-5 Precursor methane retrieval (issue 1.10), SRON-S5P-LEV2-RP-001" (SRON, 2019).
41. J.-X. Sheng, D. J. Jacob, J. D. Maasakkers, Y. Zhang, M. P. Sulprizio, Comparative analysis of low-Earth orbit (TROPOMI) and geostationary (GeoCARB, GEO-CAPE) satellite instruments for constraining methane emissions on fine regional scales: Application to the Southeast US. *Atmos. Meas. Tech.* **11**, 6379–6388 (2018).
42. G. P. Brasseur, D. J. Jacob, *Modeling of Atmospheric Chemistry* (Cambridge Univ. Press, 2017).
43. C. L. Heald, D. J. Jacob, D. B. A. Jones, P. I. Palmer, J. A. Logan, D. G. Streets, G. W. Sachse, J. C. Gille, R. N. Hoffman, T. Nehrkorn, Comparative inverse analysis of satellite (MOPITT) and aircraft (TRACE-P) observations to estimate Asian sources of carbon monoxide. *J. Geophys. Res. Atmos.* **109**, D23306 (2004).
44. D. H. Cusworth, D. J. Jacob, J.-X. Sheng, J. Benmergui, A. J. Turner, J. Brandman, L. White, C. A. Randles, Detecting high-emitting methane sources in oil/gas fields using satellite observations. *Atmos. Chem. Phys.* **18**, 16885–16896 (2018).
45. M. M. Rienecker, M. J. Suarez, R. Todling, J. Bacmeister, L. Takacs, H.-C. Liu, W. Gu, M. Sienkiewicz, R. D. Koster, R. Gelaro, I. Stajner, J. E. Nielsen, "The GEOS-5 data assimilation system—Documentation of versions 5.0.1, 5.1.0, and 5.2.0" (NASA Tech. Rep. NASA/TM-2008-104606, NASA, 2008), vol. 27, 118 pp.; https://gmao.gsfc.nasa.gov/pubs/docs/Rienecker369.pdf.
46. E. J. Dlugokencky, A. M. Crotwell, P. M. Lang, J. W. Mund, M. E. Rhodes, Atmospheric methane dry air mole fractions from quasi-continuous measurements at Barrow, Alaska and Mauna Loa, Hawaii, 1986–2017, version: 2019-06-21; ftp://aftp.cmdl.noaa.gov/data/trace_gases/ch4/in-situ/surface/ (2018).
47. A. E. Andrews, J. D. Kofler, M. E. Trudeau, J. C. Williams, D. H. Neff, K. A. Masarie, D. Y. Chao, D. R. Kitzis, P. C. Novelli, C. L. Zhao, E. J. Dlugokencky, P. M. Lang, M. J. Crotwell, M. L. Fischer, M. J. Parker, J. T. Lee, D. D. Baumann, A. R. Desai, C. O. Stanier, S. F. J. De Wekker, D. E. Wolfe, J. W. Munger, P. P. Tans, CO_2, CO, and CH_4 measurements from tall towers in the NOAA Earth System Research Laboratory's Global Greenhouse Gas Reference Network: Instrumentation, uncertainty analysis, and recommendations for future high-accuracy greenhouse gas monitoring efforts. *Atmos. Meas. Tech.* **7**, 647–687 (2014).

48. C. Sweeney, A. Karion, S. Wolter, T. Newberger, D. Guenther, J. A. Higgs, A. E. Andrews, P. M. Lang, D. Neff, E. Dlugokencky, J. B. Miller, S. A. Montzka, B. R. Miller, K. A. Masarie, S. C. Biraud, P. C. Novelli, M. Crotwell, A. M. Crotwell, K. Thoning, P. P. Tans, Seasonal climatology of CO_2 across North America from aircraft measurements in the NOAA/ESRL Global Greenhouse Gas Reference Network. *J. Geophys. Res. Atmos.* **120**, 5155–5190 (2015).
49. J. D. Maasakkers, D. J. Jacob, M. P. Sulprizio, A. J. Turner, M. Weitz, T. Wirth, C. Hight, M. DeFigueiredo, M. Desai, R. Schmeltz, L. Hockstad, A. A. Bloom, K. W. Bowman, S. Jeong, M. L. Fischer, Gridded national inventory of U.S. methane emissions. *Environ. Sci. Technol.* **50**, 13123–13133 (2016).
50. Enverus DrillingInfo, DI Desktop (2019); didesktop.com.
51. EPA, Inventory of US greenhouse gas emissions and sinks: 1990–2014 (2016); https://www.epa.gov/ghgemissions/inventory-us-greenhouse-gas-emissions-and-sinks-1990-2014.
52. EDF, New Mexico oil & gas data (2019); https://www.edf.org/nm-oil-gas/ [accessed 18 August 2019].
53. A. J. Marchese, T. L. Vaughn, D. J. Zimmerle, D. M. Martinez, L. L. Williams, A. L. Robinson, A. L. Mitchell, R. Subramanian, D. S. Tkacik, J. R. Roscioli, S. C. Herndon, Methane emissions from United States natural gas gathering and processing. *Environ. Sci. Technol.* **49**, 10718–10727 (2015).
54. A. L. Mitchell, D. S. Tkacik, J. R. Roscioli, S. C. Herndon, T. I. Yacovitch, D. M. Martinez, T. L. Vaughn, L. L. Williams, M. R. Sullivan, C. Floerchinger, M. Omara, R. Subramanian, D. Zimmerle, A. J. Marchese, A. L. Robinson, Measurements of methane emissions from natural gas gathering facilities and processing plants: Measurement results. *Environ. Sci. Technol.* **49**, 3219–3227 (2015).
55. C. Elvidge, M. Zhizhin, K. Baugh, F.-C. Hsu, T. Ghosh, Methods for global survey of natural gas flaring from visible infrared imaging radiometer suite data. *Energies* **9**, 14 (2016).
56. A. M. Robertson, R. Edie, D. Snare, J. Soltis, R. A. Field, M. D. Burkhart, C. S. Bell, D. Zimmerle, S. M. Murphy, Variation in methane emission rates from well pads in four oil and gas basins with contrasting production volumes and compositions. *Environ. Sci. Technol.* **51**, 8832–8840 (2017).
57. D. Zavala-Araiza, D. R. Lyon, R. A. Alvarez, K. J. Davis, R. Harriss, S. C. Herndon, A. Karion, E. A. Kort, B. K. Lamb, X. Lan, A. J. Marchese, S. W. Pacala, A. L. Robinson, P. B. Shepson, C. Sweeney, R. Talbot, A. Townsend-Small, T. I. Yacovitch, D. J. Zimmerle, S. P. Hamburg, Reconciling divergent estimates of oil and gas methane emissions. *Proc. Natl. Acad. Sci. U.S.A.* **112**, 15597–15602 (2015).